THE JOURNAL OF BIOLOGICAL CHEMISTRY
Vol. 277, No. 45, Issue of November 8, pp. 43033–43040, 2002
Printed in U.S.A.

Structure of a Novel P-superfamily Spasmodic Conotoxin Reveals an Inhibitory Cystine Knot Motif*[S]

Received for publication, July 5, 2002, and in revised form, August 16, 2002
Published, JBC Papers in Press, August 21, 2002, DOI 10.1074/jbc.M206690200

Luke A. Miles‡§, Catherine Y. Dy¶‖, Jake Nielsen, Kevin J. Barnham§‡‡, Mark G. Hinds‡, Baldomero M. Olivera¶, Grzegorz Bulaj¶** and Raymond S. Norton‡§¶¶**

*From the ‡The Walter and Eliza Hall Institute of Medical Research, NMR Laboratory, 381 Royal Parade, Parkville 3052, Australia, §Biomolecular Research Institute, 343 Royal Parade, Parkville 3052, Australia, ¶Department of Biology, University of Utah, Salt Lake City, Utah 84112, ‖Marine Science Institute, University of the Philippines, Diliman, Quezon City 1101, The Philippines, **Cognetix Incorporated, Salt Lake City, Utah 84108, and ‡‡Department of Pathology, The University of Melbourne, Parkville 3010, Australia*

Conotoxin gm9a, a putative 27-residue polypeptide encoded by *Conus gloriamaris*, was recently identified as a homologue of the "spasmodic peptide", tx9a, isolated from the venom of the mollusk-hunting cone shell *Conus textile* (Lirazan, M. B., Hooper, D., Corpuz, G. P., Ramilo, C. A., Bandyopadhyay, P., Cruz, L. J., and Olivera, B. M. (2000) *Biochemistry* 39, 1583–1588). The *C. gloriamaris* spasmodic peptide has been synthesized, and the refolded polypeptide was shown to be biologically active using a mouse bioassay. The chemically synthesized gm9a elicited the same symptomatology described previously for natively folded tx9a, and gm9a and tx9a were of similar potency, implying that neither the two γ-carboxyglutamate (Gla) residues found in tx9a (Ser^8 and Ala^{13} in gm9a) nor Gly^1 (Ser^1 in gm9a) are crucial for biological activity. We have determined the three-dimensional structure of gm9a in aqueous solution and demonstrated that the molecule adopts the well known inhibitory cystine knot motif constrained by three disulfide bonds involving Cys^2-Cys^{16}, Cys^6-Cys^{18} and Cys^{12}-Cys^{23}. Based on the gm9a structure, the sites of Gla substitution in tx9a are in loops located on one surface of the molecule, which is unlikely to be involved directly in receptor binding. Because this is the first structure reported for a member of the newly defined P-superfamily conotoxins, a comparison has been made with structurally related conotoxins. This shows that the structural scaffold that characterizes the P-conotoxins has the greatest potential for exhibiting structural diversity among the robust inhibitory cystine knot-containing conotoxins, a finding that has implications for functional epitope mimicry and protein engineering.

A novel *Conus* polypeptide was recently purified and characterized from the venom of *Conus textile*, a *Conus* species known to hunt other snails (1). The new polypeptide defined a new class of venom components, the P-conotoxin superfamily, which has a distinctive cysteine framework, -$CX_3CX_5CX_3$-$CXCX_4C$-, where *X* can be any amino acid. Conopeptides with three disulfide linkages and no half-cystines adjacent to each other have not been characterized previously (1, 2). The polypeptide purified from *C. textile* venom designated the "spasmodic peptide" is unusual in two respects. First, when injected into mice it phenocopied a well known mutant, the spasmodic mouse (3, 4). Second, in addition to the standard amino acids, this polypeptide has two residues of γ-carboxyglutamate (Gla),[1] a distinctive post-translationally modified amino acid.

A second member of the P-superfamily was identified by molecular techniques from a different *Conus* species, *Conus gloriamaris*. The sequence of the latter was inferred from a cDNA clone (1). The predicted mature *C. gloriamaris* sequence is largely identical to the *C. textile* spasmodic peptide sequence, but it does not have the two glutamate codons presumably encoding Glu residues post-translationally modified to Gla. This polypeptide has not yet been isolated from *C. gloriamaris* venom. The sequences of the two mature P-superfamily polypeptides are shown in Fig. 1.

In this work, we have synthesized and refolded the *C. gloriamaris* polypeptide, gm9a, and assessed its activity in the same bioassay used to characterize tx9a. This has been done as a first step in understanding the molecular basis of the symptomatology elicited by tx9a, which is unique among known conotoxins. Of particular interest is the significance of the post-translationally modified amino acids found in tx9a but not in gm9a. Further to this end, we have determined the three-dimensional structure of gm9a in aqueous solution, which is expected to be homologous to that of tx9a considering the extent of sequence homology between the two polypeptides.

Because of their small size, robustness, and scope for structural diversity, conotoxins can be regarded as scaffolds that can be engineered for the mimicry of functional epitopes (5). In this context, the structures of the P-conotoxins are of interest because of their novel cysteine framework. In this work, we explore the structural consequences of the additional degrees of freedom in the molecular structure that result when no Cys

* The work at the University of Utah was supported by Grant GM48677 from NIGMS, National Institutes of Health (to B. M. O.). The costs of publication of this article were defrayed in part by the payment of page charges. This article must therefore be hereby marked "*advertisement*" in accordance with 18 U.S.C. Section 1734 solely to indicate this fact.

[S] The on-line version of this article (available at *http://www.jbc.org*) contains Tables SI, SII, SIII, and SIV.

The atomic coordinates and structure factors (code 1IXT) have been deposited in the Protein Data Bank, Research Collaboratory for Structural Bioinformatics, Rutgers University, New Brunswick, NJ (http://www.rcsb.org/).

The nucleotide sequence(s) reported in this paper has been submitted to the GenBank™/EBI Data Bank with accession number(s) AF193510 and AF193511.

¶¶ To whom correspondence should be addressed: The Walter and Eliza Hall Institute of Medical Research, NMR Laboratory, 381 Royal Parade, Parkville 3052, Australia. Tel.: 61-3-9903-9650; Fax: 61-3-9903-9655; E-mail: Ray.Norton@wehi.edu.au.

[1] The abbreviations used are: Gla, γ-carboxyglutamate; Fmoc, *N*-(9-fluorenyl)methoxycarbonyl; TCEP, Tris-[2-carboxyethyl]phosphine hydrochloride; HPLC, high performance liquid chromatography; ICK, inhibitory cystine knot; NOE, nuclear Overhauser effect.

residues are directly adjacent in the polypeptide sequence. The gm9a structure is considered in comparison with structurally related conotoxins, particularly the well characterized O-superfamily conotoxins (6, 7).

EXPERIMENTAL PROCEDURES

Peptide Synthesis and Folding—Peptides were synthesized using standard solid-phase Fmoc protocol and standard side chain protections. The polypeptides were cleaved from solid support using reagent K (trifluoroacetic acid:water:ethanedithiol:phenol:thioanisole, 90:5:2.5:7.5:5 by volume, respectively) for 3 h at room temperature. The crude polypeptide was precipitated with cold methyl *tert*-butyl ether and washed three times with methyl *tert*-butyl ether. The linear form was purified using semi-preparative reversed-phase C18 HPLC. The identity of the linear polypeptide was confirmed by electrospray ionization mass spectrometry. Folding reactions were carried out at 0 °C and contained 0.1 M Tris-HCl, 0.1 mM EDTA, 1 mM oxidized glutathione, 2 mM reduced glutathione, pH 8.7, and 20 μM linear polypeptide. After 24 h, the reaction was quenched by adding formic acid to 5% final concentration, and the mixture was separated by reversed-phase C18 HPLC in a linear gradient of acetonitrile in 0.1% trifluoroacetic acid from 9 to 31.5% in 20 min. For analytical and semi-preparative C18 columns, flow rates of 1 and 5 ml/min were used, respectively. All HPLC chromatography was monitored using absorbance at 220 nm.

NMR Spectroscopy—A sample of gm9a was prepared for NMR analysis by dissolving the polypeptide in 0.30 ml of 90% H_2O, 10% ^2H_2O. The pH was adjusted to 5.5 with small additions of 0.5 M NaO^2H, and the solution was transferred to a ^2H_2O-matched Shigemi tube (5-mm-outer diameter, 8-mm-bottom length). Reported pH values were recorded at room temperature with no correction made for isotope effects. ^1H chemical shifts were referenced to 2,2-dimethyl-2-silapentane-5-sulfonate at 0 ppm via the chemical shift of 1,4-dioxane at 3.75 ppm (8).

NMR spectra were recorded on Bruker AMX-500 or DRX-600 spectrometers. All two-dimensional spectra were recorded in phase-sensitive mode using the time-proportional phase incrementation method (9). Water suppression was achieved either by pulsed field gradients employing the Watergate method of Sklenar *et al.* (10) or by selective low power irradiation of the water signal during the relaxation delay (typically 1.8 s) and during the mixing time in NOESY experiments. Unless otherwise indicated, spectra were recorded at 5 °C. Two-dimensional homonuclear NOESY spectra (9, 11) were recorded with mixing times of 75 and 250 ms. TOCSY spectra (12) were recorded using the MLEV spin-lock sequence (13) with a spin-lock time of 70 ms. DQF-COSY (14) and E-COSY (15) spectra were also recorded. Typically, spectra were acquired with t_1 = 400–500 increments, 32–128 scans/increment, and 4096 data points. ^1H sweep-widths were 7575.8 and 8992.8 Hz at 500 and 600 MHz, respectively. Spectra were processed using XWIN-NMR, version 1.3 (Bruker) and analyzed using XEASY, version 1.3.13 (16). Sine-squared window functions, phase-shifted by 60–90°, were applied in both dimensions prior to Fourier transformation.

The $^3J_{NHC\alpha H}$ coupling constants were measured from a DQF-COSY spectrum at 500 MHz. The appropriate rows were extracted from the spectrum, inverse Fourier transformed, zero-filled to 64 K, and multiplied by a Gaussian window function prior to Fourier transformation.

The temperature dependence of each amide proton chemical shift was determined from one-dimensional spectra, recorded over the temperature range of 5–30 °C. Slowly exchanging amide protons in the polypeptide were identified by dissolving the lyophilized polypeptide in ^2H_2O (99.96% ^2H, Cambridge Isotope Laboratories) at pH 5.5 and 5 °C and recording a series of one-dimensional and TOCSY spectra over 48 h. The chemical shifts of pH-dependent protons were monitored in a pH titration with TOCSY and one-dimensional spectra recorded at several values of pH in the range of 3.7–8.5 and 5 °C.

Structural Constraints—Upper bound distance constraints were calculated from cross-peak volumes observed in a NOESY spectrum recorded with a 250-ms mixing time. These distance constraints were calibrated with the use of the CALIBA macro invoked in the torsion angle dynamics program DYANA (17) with volumes proportional to r^{-6} for distances involving backbone protons and r^{-4} for all other distances. Distance constraints involving backbone atoms were loosened by a factor of 1.2 to allow for spin diffusion.

Backbone dihedral angle constraints were inferred from $^3J_{NHC\alpha H}$ values as follows: $^3J_{NHC\alpha H} < 6$ Hz, $\phi = -60 \pm 30°$; $^3J_{NHC\alpha H} > 8$ Hz, $\phi = -120 \pm 30°$. Where possible, $^3J_{C\alpha HC\beta H}$ coupling constants were measured from passive couplings as displacements in an E-COSY spectrum. The relative intensities of intra-residue $d_{\alpha\beta}(i,i)$ and $d_{N\beta}(i,i)$ NOEs were measured in a 75-ms mixing time NOESY spectrum. These $^3J_{C\alpha HC\beta H}$ coupling constants and NOE intensities were used to determine whether side chains could be placed in one of the three-staggered side-chain rotamer conformations ($\chi^1 = -60$, 60, or 180°) and to make stereospecific assignments.

Preliminary Structure Calculations—Preliminary structure calculations were performed in DYANA to facilitate the assignment of ambiguous NOE cross-peaks and to refine distance constraints. 200 structures were calculated from the refined list of structural constraints excluding disulfide bonds. To elucidate the disulfide connectivities in gm9a, these calculations were repeated with each possible combination of cysteine pairings constrained. The 20 lowest energy structures obtained from each series of calculations were selected, and each family of structures was assessed on the extent to which they violated the NMR data. Prior to further refinement of the structures, disulfide-bond connectivities were confirmed by chemical means (described below).

Structure Refinement and Analysis—Final structural calculations were performed in the CNS software suite (18) with disulfide bonds constrained. 200 structures were calculated in CNS via distance geometry, simulated annealing, and low temperature-simulated annealing. The structures obtained were then energy minimized in a box of water using the OPLSX parameter set of Linge and Nilges (19). 20 structures were selected from 200 water-minimized structures on the basis of lowest energy terms associated with violation of experimentally derived constraints. Procheck (20) was used to identify elements of secondary structure in gm9a and to construct a Ramachandran plot of φ/ψ angles in the family of 20 structures.

Verification of Disulfide Connectivities—To determine the pairing of Cys residues forming native disulfide bonds, we used the strategy described by Gray (21). An equal volume of 20 mM TCEP (Pierce, Rockford, IL) in 0.2 M citrate buffer, pH 3.0, and folded gm9a in HPLC eluent were mixed and allowed to react for 20 min at room temperature. Typically, the reaction contained 5–10 nmol of polypeptide in 0.1–0.2 ml. Resulting products were separated by reversed-phase HPLC using analytical C18 column (Vydac) in a linear gradient of acetonitrile (in 0.1% trifluoroacetic acid) from 13.5% to 22.5% in 20 min. The HPLC peaks were immediately subjected to rapid alkylation using saturated iodoacetamide solution. The iodoacetamide (0.1 g) was dissolved in 0.2 ml of 0.5 M Tris acetate buffer, 2 mM EDTA, pH 8.0, and the solution was heated to 65 °C until the solid was dissolved. 10 μl of 100 mM ascorbic acid was added to the iodoacetamide solution to scavenge possible traces of iodine, and then 0.3 ml of the partially reduced intermediate in HPLC eluent was rapidly injected into the cooled iodoacetamide solution using a fine-tipped syringe and mixed vigorously for 30 s. The alkylation was then quenched with 0.5 M citric acid (0.4 ml), and the mixture was separated on a C18 analytical HPLC column. The following elution conditions were developed to separate alkylation products: 20 min of 9% acetonitrile in 0.1% trifluoroacetic acid (isocratic) followed by a linear gradient of acetonitrile (9–45% for 20 min) and flow rate of 1 ml/min. The resulting disulfide intermediates, which contained some pairs of carboxymethylated Cys residues, were further reduced with dithiothreitol and alkylated with 4-vinylpyridine. The HPLC eluent containing the intermediates was adjusted to pH 8.0 by adding 0.5 M Tris base solution. The intermediates were reduced in 10 mM dithiothreitol at 65 °C for 15 min. After the solution was cooled, 3 μl of 4-vinylpyridine was added for every 0.5 ml of the sample volume. The alkylation reaction was carried out in the dark at room temperature for 25 min and then diluted with 0.1% trifluoroacetic acid and injected on a C18 analytical HPLC column. The HPLC conditions were similar to those described above with the exception of the linear acetonitrile gradient applied (9–27% in 20 min). The final alkylation products were sequenced using a standard Edman protocol. Positions of carboxymethylated and pyridylethylated cysteines were determined from the sequencing data.

RESULTS

Chemical Synthesis of gm9a—To further define the newly elucidated P-superfamily (1), we chemically synthesized and folded conotoxin gm9a (sequences in Fig. 1) also called the *C. gloriamaris* spasmodic peptide. The biologically active conotoxin was first synthesized as a linear chain using standard Fmoc protocol. Cleavage and deprotection was achieved by incubating resin with reagent K as specified under "Experimental Procedures." The linear form was purified using semi-preparative reversed-phase C18 HPLC. The identity of the synthetic polypeptide was confirmed by electrospray-ionization mass spectroscopy.

		5 10 15 20 25
Conus textile	tx9a	GCNNSCQγHSDCγSHCICTFRGCGAVN#
Conus gloriamaris	gm9a	SCNNSCQSHSDCASHCICTFRGCGAVN#

FIG. 1. **Amino acid sequences tx9a and gm9a.** Sequences of the tx9a and gm9a polypeptides from *C. textile* and *C. gloriamaris*, respectively (GenBank™ accession numbers AF193510 and AF193511, respectively). In the tx9a sequence, γ represents the non-standard amino acid Gla. The locations of disulfide bonds determined in this paper are indicated.

To obtain a cyclic polypeptide with disulfide bridges, we used a direct oxidation method in which the polypeptide containing six unprotected cysteines was allowed to form disulfides under oxidizing conditions. The linear polypeptide was treated with the mixture of oxidized and reduced glutathione. The folding reaction contained 0.1 M Tris-HCl, 0.1 mM EDTA, 1 mM oxidized glutathione, 2 mM reduced glutathione, pH 8.7, and linear polypeptide (20 μM). Folding was carried out at 0 °C for 24 h. The acid-quenched reaction mixture was separated by reversed-phase C18 HPLC. A major folding product was purified and characterized using the mouse bioassay previously employed for the *C. textile* spasmodic peptide (1). Qualitatively, the biological activity of purified synthetic gm9a was similar to that described previously for tx9a, the spasmodic peptide isolated from the venom of *C. textile* (1). Both peptides elicited the spasmodic symptomatology described previously (1). A direct comparison between the two peptides demonstrated that both caused hypersensitivity to touch in mice when injected at a dose of 2 nmol and hyperactivity and convulsions at 5 nmol.[2]

NMR Spectroscopy—NMR spectra for structural analysis were collected on the gm9a polypeptide in 90% H_2O, 10% ^2H_2O at pH 5.5. Broad NH chemical shift dispersion in one-dimensional spectra indicated that the polypeptide was well structured, and standard two-dimensional spectra recorded at 5, 15, and 25 °C showed that only one conformation was present in aqueous solution at these temperatures. Most amide peaks were well resolved at all of these temperatures, and many values of the $^3J_{NHC\alpha H}$ coupling constants were apparent from the one-dimensional spectra at 500 MHz. Sequence-specific chemical shift assignments were made at 600 MHz for backbone and side-chain protons in gm9a with the aid of standard two-dimensional homonuclear NMR experiments. These assignments are provided as supplementary data (Table S-I) and have been deposited with BioMagResBank (22) under accession number BMRB-6086. Distance constraints were taken from the volumes of NOE cross-peaks in NOESY spectra acquired at 5 °C at 600 MHz.

In general, spectral overlap was minimal, but overlap in the regions of the Cys $C^\beta H$ and NH resonances made it difficult to assign unambiguously a small number of NOE cross-peaks that might have assisted in the identification of Cys-Cys bonds. Most of these ambiguities were resolved by conducting experiments at different temperatures and different pH values to disperse chemical shifts of key protons. Despite this, direct identification of Cys-Cys connectivities remained problematic as a number of Cys $C^\alpha H$ and $C^\beta H$ had through-space NOE cross-peaks with more than one other Cys, indicative of a cluster of Cys side-chains in the polypeptide.

A suite of NMR experiments yielded distance and torsion angle constraints for use in structural calculations. Initial calculations were performed in DYANA with no disulfide or hydrogen bonds present. The family of 20 best structures obtained with no disulfide bonds imposed was used as a reference to determine the disulfide-bonding pattern in gm9a that was most consistent with the NMR data.

[2] E. C. Jimenez, unpublished results.

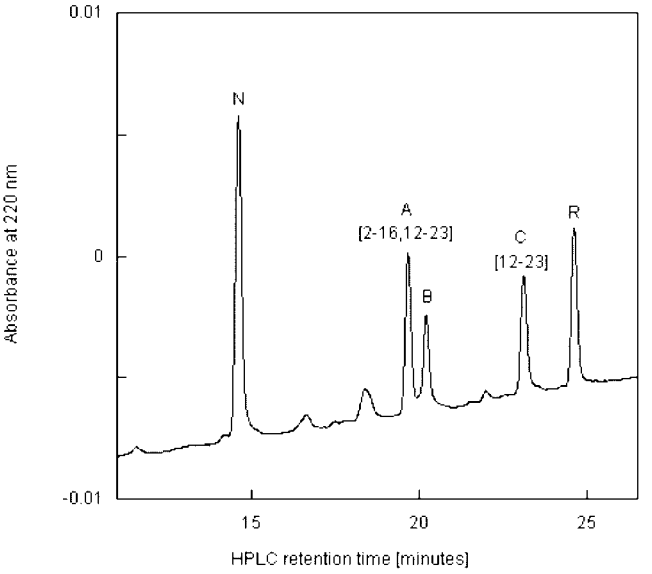

FIG. 2. **Chemical verification of disulfide connectivity in gm9a.** The folded gm9a was partially reduced using 20 mM TCEP at pH 3.0 for 20 min and separated by reversed-phase HPLC. The disulfide connectivities of resulting intermediates were determined by differential alkylation of Cys thiols with iodoacetamide and 4-vinylpyridine followed by Edman sequencing. Peaks labeled *N* and *R* correspond to the folded and fully reduced forms, respectively. Intermediates *A* and *C* are shown with their deduced disulfide connectivity. Intermediate *B* could not be further analyzed because of intramolecular rearrangement during alkylation of thiols. The minor peaks between N and A arise from reagent contamination. Experimental details of reduction and alkylation are described under "Experimental Procedures."

Structural constraints were well satisfied for every combination involving either the Cys^2-Cys^{16} or Cys^6-Cys^{18} pairings (Table S-II from supplementary data), and the lowest target function was obtained when both of these bonds were in place, *i.e.* the combination of Cys^2-Cys^{16}, Cys^6-Cys^{18}, and Cys^{12}-Cys^{23}. The structures derived with this combination of disulfides used to constrain the molecule showed that gm9a adopts the inhibitory cystine knot (ICK) motif (7, 23), a common structural motif incorporating a cystine knot and a triple-stranded β-sheet in toxic and inhibitory polypeptides.

Chemical Verification of Disulfide Connectivity in gm9a—The disulfide connectivities consistent with the NMR data were confirmed chemically before the final structure calculations were undertaken. The general strategy involved a partial reduction of the folded gm9a at acidic pH followed by a primary alkylation of the resulting Cys thiols with iodoacetamide. The alkylation products were isolated by reversed-phase HPLC, further reduced with dithiothreitol, and subjected to a secondary alkylation with 4-vinylpyridine. The Cys connectivities were deduced using standard Edman sequencing by identification of positions of carboxymethyl- and pyridylethyl-modified cysteines.

Fig. 2 shows the HPLC separation of products after TCEP reduction of the folded gm9a for 20 min at pH 3.0. Three major intermediates were purified and alkylated with iodoacetamide as described under "Experimental Procedures." Two intermediates (Fig. 2, peaks labeled *A* and *C*) yielded clear alkylation products. However, intermediate B apparently underwent a rearrangement during alkylation as judged by multiple alkylation products observed after HPLC analysis (data not shown). Therefore, only alkylated intermediates A and C were further purified using reversed-phase HPLC.

The polypeptides were reduced for 15 min at 65 °C using 10 mM dithiothreitol followed by addition of 4-vinylpyridine. After secondary alkylation, the polypeptides were purified by HPLC and sequenced. Intermediate A contained carboxymethylated cysteines at positions 6 and 18 and pyridylethylated cysteines at positions 2, 12, 16, and 23. Intermediate C contained carboxymethylated cysteines at positions 2, 6, 16, and 18 and pyridylethylated cysteines at positions 12 and 23. Based on these data, we deduce that the disulfide connectivity of biologically active gm9a is Cys^2-Cys^{16}, Cys^6-Cys^{18}, and Cys^{12}-Cys^{23}, which is the combination most consistent with the NMR data.

NMR Assessment of Hydrogen Bonds—The temperature dependence of the chemical shift of each gm9a amide proton was determined to probe for hydrogen bonding. However, all amide protons exhibiting a temperature coefficient of magnitude ≤3 ppb/°C (Table S-III from supplementary data) were found to be from either cysteines (16, 18, 23) or residues directly adjacent to cysteines (5, 7, 11, 24). Because structure calculations indicated that the three disulfides form the core of folded gm9a, the low susceptibility of these amide chemical shifts to a change in temperature presumably reflects the location of these protons in the polypeptide core rather than their involvement in hydrogen bonding (24). Amide exchange experiments conducted at 5 °C and pH 5.5 indicated that all amide protons with the exception of those of Gln^7 and Ile^{17} exchanged with solvent deuterium within minutes of dissolution of the polypeptide in ^2H_2O. Amide protons from these two residues were apparent in NMR spectra for several hours following dissolution; however, again these residues are directly adjacent to core Cys residues. Because the experimental indicators of hydrogen bonding could have been influenced by reduced solvent accessibility, no hydrogen bonds were used as distance constraints in structural calculations.

Solution Structure of Conotoxin gm9a—Parameters characterizing the final 20 structures of gm9a and structural statistics are summarized in Table I, and stereoviews of the structures superimposed over the backbone are shown in Fig. 3. These structures were calculated with the chemically determined disulfide bonds intact. Table I indicates that the final 20 structures fit well with experimentally derived distance and angle constraints and are well defined over the entire length of the polypeptide. The structures of gm9a have been deposited with the Protein Data Bank (PDB accession number 1IXT) (25).

Different features of the closest-to-mean gm9a structure are highlighted in Fig. 4. In terms of overall topology, the molecule has a sulfur-rich core of three disulfides that form an inhibitory cystine knot as illustrated in Fig. 4*E* and a backbone made up of three extended sections encompassing residues 1–6, 15–19, and 22–27 and three loops centered on residues 7–11, 12–14, and 20–21. Procheck (20) was used to identify elements of secondary structure in the final family of gm9a structures. The most prominent feature of the structures is a β-hairpin in the COOH-terminal half of the molecule (Fig. 4, *A* and *B*) with the first extended β-strand encompassing His^{15}-Thr^{19}, and the second extended β-strand encompassing Gly^{22}-Ala^{26}. The loop at the center of the hairpin (Phe^{20} and Arg^{21}) was identified as a hydrogen-bond-stabilized Type I turn. Procheck also identified an isolated β-bridge at Asn^4 that is hydrogen-bonded through its carbonyl to Cys^{23} in the second β-strand (26). However, all of the residues in the range Cys^2-Cys^6 occupied the β-sheet region of the Ramachandran plot, suggesting that gm9a contains a triple-stranded anti-parallel β-sheet in common with many ICK-containing conopeptides (7). The fact that this extended region is constrained at either end by a disulfide-bonded Cys (Cys^2 and Cys^6) may distort the backbone from ideal β-strand geometry. The final structures also contain hydrogen bonds between strands and across all three loops (Table S-III from supplementary data). The disulfides formed by Cys^2-Cys^{16} and Cys^{12}-Cys^{23} adopt a left-handed conformation, whereas the remaining disulfide, Cys^6-Cys^{18}, is right-handed.

TABLE I
Structural statistics for gm9a

No. of NOE-derived distance constraints	
Total	439
Intraresidual and sequential	242
Medium range	30
Long range backbone	12
Long range	137
No. of dihedral angle constraints	26
No. of φ angle constraints	23
No. of χ^1 angle constraints	3
Constraint violations	
No. of distance violations > 0.2 Å	0
No. of dihedral violations > 5 °	0
r.m.s. deviations from experimental constraints[a,b]	
439-interproton distance constraints (Å)	0.025 ± 0.001
26 dihedral angle constraints (°)	0.554 ± 0.174
r.m.s. deviations from idealized geometry	
Bonds (Å)	0.0048 ± 0.0002
Angles (°)	0.481 ± 0.046
Impropers (°)	0.373 ± 0.053
Backbone atoms r.m.s. deviations (Å)[c]	0.70 ± 0.17
All heavy atoms r.m.s. deviations (Å)[d]	1.30 ± 0.18
Ramachandran plot	
% in favored region	56.5
% in additionally allowed region	30.4
% in generously allowed region	13.0

[a] Average values ± S.D. calculated for the 20 final structures.
[b] Best values for the 20 final structures.
[c] Average pairwise r.m.s. deviations of atomic coordinates C′, C^α, and N for residues 1–27 across the 20 final structures.
[d] Average pairwise r.m.s. deviations of all atoms excluding hydrogen for residues 1–27 across the 20 final structures.

gm9a contains only three charged residues at physiological pH, namely Asp^{11}, Arg^{21}, and the protonated N terminus, Ser^1. As illustrated in Fig. 4, *C* and *D*, the positively charged centers on Ser^1 and Arg^{21} are in close proximity to each other on one face of the molecule, and the negatively charged Asp^{11} is on the opposite face. Fig. 4*F* shows the distribution of hydrophobic residues in gm9a, which occur principally on the same face as the cationic residues and on the opposite face to Asp^{11}, which is located on a surface composed mainly of polar residues. Also shown is the location of the Gla substitutions (Ser^8 and Ala^{13}) in tx9a, which are situated on the Asp^{11} face of the molecule.

An unexpected feature of the spectra was a broad peak at 11.3 ppm in one- and two-dimensional spectra recorded at pH 5.5. This resonance showed NOESY cross peaks to side-chain protons on Ile^{17} and Cys^{18}. Spectra recorded over a range of pH showed that the chemical shift and line width of this peak were highly dependent on pH, indicating that the proton was in exchange with solvent protons. An analysis of the final structures indicate that the only exchangeable peak in sufficiently close proximity to the side-chains of Ile^{17} and Cys^{18} is the imidazole proton of His^9. This is supported by its chemical shift, which is consistent with that of a His side-chain NH (22, 27).

A limited pH titration was undertaken to determine the pK_a values for the imidazolium groups of His^9 and His^{15} and the carboxyl of Asp^{11}. As summarized in Table S-IV from supplementary data, the imidazolium pK_a values were 4.9 and 6.0, respectively, and the carboxyl pK_a value was 4.8. In small histidine-containing peptides the imidazolium pK_a was 7.0 at 35 °C (28), whereas in the uncharged model compound Ac-His-NHMe, it was 6.38 at 37 °C (29), 6.43 in H_2O, and 6.54 in ^2H_2O, each containing 0.1 M NaCl at 30 °C (30). The intrinsic pK_a cited by Shire *et al.* (31) is 6.3. The pK_a of His^{15} is only slightly

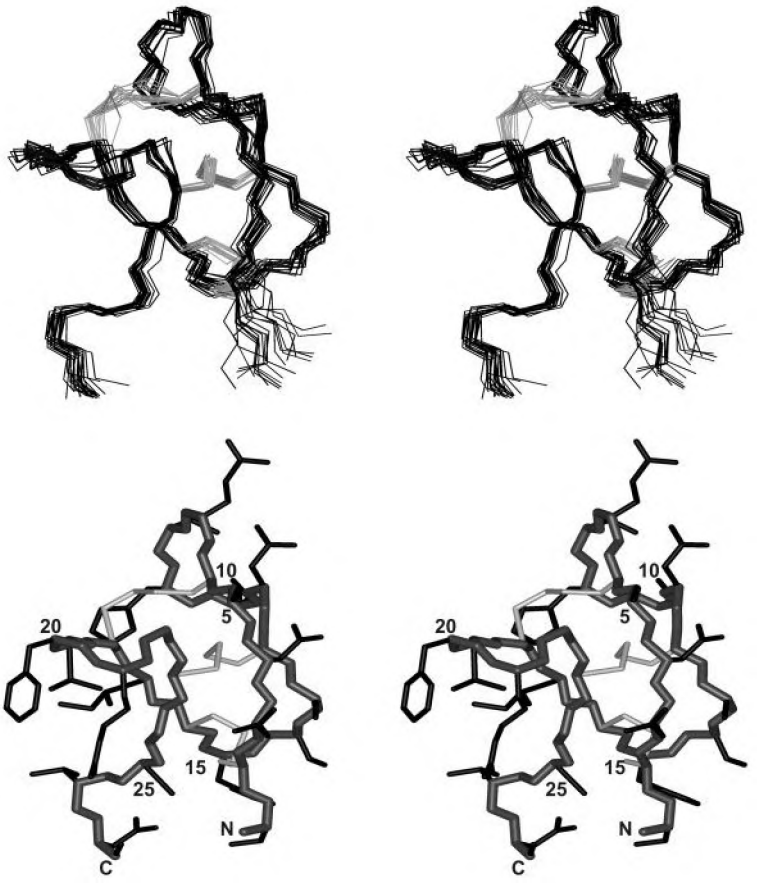

FIG. 3. **gm9a structures.** Stereoviews of the family of 20 final structures determined for gm9a superimposed over backbone heavy atoms from all 27 residues. For clarity, amino acid side-chains have been eliminated from the family of structures in the *top view*. Side-chain orientations are shown for the closest-to-mean structure in the *bottom view*. Disulfide bonds are shown in *gray*. The letters *N* and *C* refer to the amino and carboxyl termini, respectively.

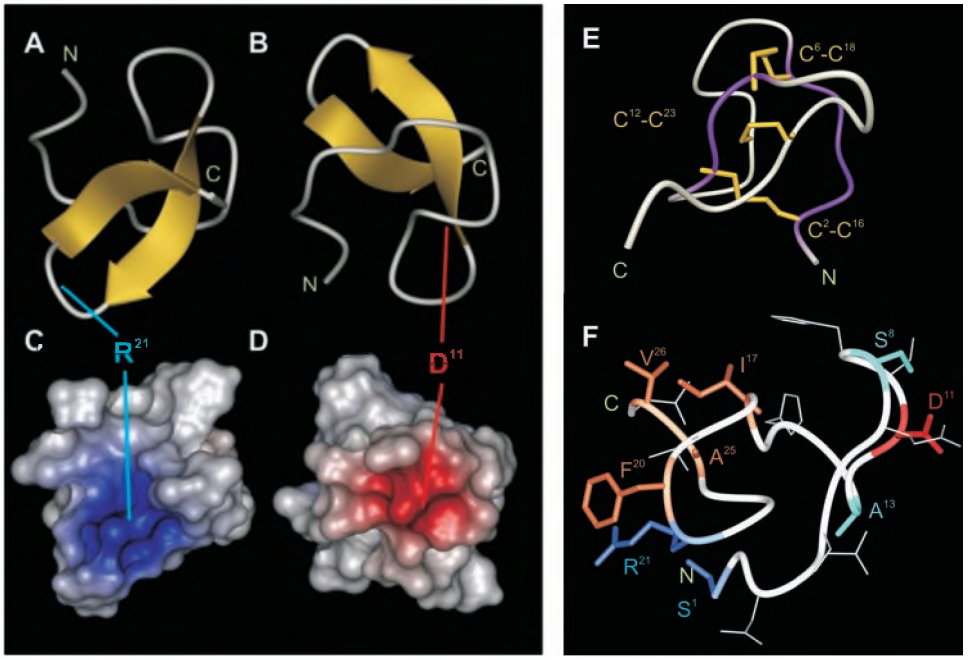

FIG. 4. **Aspects of the gm9a structure.** *A* and *B*, *ribbon diagrams* representing the closest-to-mean gm9a structure where the two perspectives are related by a 180° rotation along the *y* axis, and *yellow arrows* indicate β-strands. *C* and *D*, simple charge distribution on the surface of gm9a and are shown in the same orientation as *A* and *B*, respectively. Electrostatic potentials are color-coded *blue* for the positively charged residues Ser^{1} and Arg^{21} and *red* for the negatively charged residue Asp^{11}. *E*, a *ribbon* representation of the gm9a backbone, which demonstrates the inhibitory cystine knot motif where the Cys^{12}-Cys^{23} disulfide bond passes through a loop constrained by the Cys^{2}-Cys^{16} and Cys^{6}-Cys^{18} disulfides. In *E*, disulfide bonds are shown in *yellow*, and the backbone of residues forming the loop are shown in *violet*. *F*, the closest-to-mean structure obtained for gm9a with the location of Ser^{8} and Ala^{13} indicated, which are sites of Gla substitution in the tx9a polypeptide. In *F*, Arg^{21} and Ser^{1} are in *blue*, hydrophobic residues (Ile^{17}, Phe^{20}, Ala^{25}, and Val^{26}) are shown in *coral* (excluding Ala^{13}), Asp^{11} is in *red*, and the sites of Gla substitution are in *cyan*. The letters *N* and *C* refer to the amino and carboxyl termini, respectively.

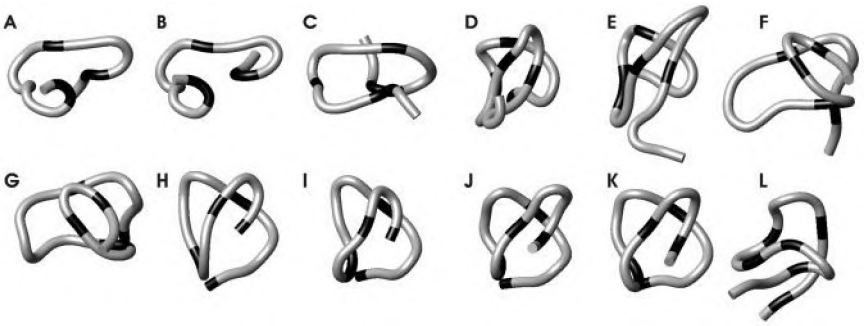

FIG. 5. **Experimental structures of conotoxins with the same disulfide-bonding pattern as gm9a.** *A–L*, smoothed *ribbon* representations of the backbone of experimentally derived conotoxin structures. The amino acid sequences corresponding to these structures are given in Table II. The structures were downloaded from the Protein Data Bank (25) and correspond as follows: *A*, GIIIB (34); *B*, GIIIA (35); *C*, ψ-PIIIE (36); *D*, TVIIA, (37); *E*, conotoxin GS (38); *F* and *G*, *trans*- and *cis*-isomers of EVIA, respectively (PDB codes 1G1P/1G1Z); *H*, SO3 (PDB code 1FYG); *I*, MVIIA (41); *J*, GVIA (42); *K*, PVIIA (43); and *L*, gm9a. The location of each cysteine is indicated in *black*.

lower than the model values, consistent with its largely solvent-exposed environment. The significantly lower pK_a for His^9 is consistent with its location on the surface but in close contact with several non-polar side chains to which it shows numerous NOEs (Ile^{17} and Cys^{18}). These interactions are expected to favor the neutral form and thus reduce the pK_a. It is probable that protonation of the imidazole side chain causes some local conformational changes associated with movement of the positively charged ring to a more solvent-exposed environment and that changes in the chemical shifts of Ile^{17} methyl resonances as this titration occurs probably reflect this. His^9 is not close to the Arg^{21} side chain or the N-terminal ammonium group, so direct effects of either of these positively charged groups are unlikely to contribute to its low pK_a.

The $C^{\beta}H$ resonances of Asp^{11} in gm9a titrate with a pK_a of 4.8 (Table S-IV from supplementary data) significantly higher than the carboxyl group of Asp in small peptides with a pK_a of 3.9 (28, 32). Even though the direction and magnitude of the chemical shift changes associated with this titration are as observed in small peptides (28), it is nevertheless possible that this pK_a reflects the titration of His^9 rather than the Asp^{11} carboxyl. The two side chains are not in close proximity; however, both residues are located on a reverse turn (distorted Type I involving His^9 and Ser^{10}), so it is possible that local conformational changes associated with the titration of His^9 could affect the environment of Asp^{11}. If the pK_a of 4.8 does reflect the carboxyl titration, then it is unusually high. As in the case of His^9, Asp^{11} is located on the surface but is in close contact with several other side chains (residues 6, 7, 8, 10, and 12) to which it shows numerous NOEs. These interactions would be expected to favor the neutral form and thereby raise the carboxyl pK_a.

DISCUSSION

Lirazan *et al.* (1) recently identified conotoxin tx9a from the venom of the cone shell *C. textile* and argued that it defined a new class of conotoxins, the P-superfamily, on the grounds that it had a novel cysteine framework (-$CX_3CX_5CX_3CXCX_4$C-) and precursor structure and was pharmacologically distinct from other conotoxins. A second polypeptide that had high sequence identity with tx9a including the distinctive Cys framework was identified in that work from *C. gloriamaris*. In this work, we have synthesized the gm9a polypeptide from *C. gloriamaris* and determined that it is pharmacologically related to tx9a. We have found these polypeptides to be indistinguishable in an *in vivo* assay in mice in which both the polypeptides phenocopy the spasmodic mouse mutant (3, 4). In this mouse, there are alterations in glycine receptors, but the molecular target of the *Conus* polypeptides in the central nervous system has not yet been determined (1).

Functional Diversity among Conotoxins—One of the tenets of structural genomics is that structure provides clues regarding function, but it has been pointed out that this nexus generally is weak in the case of polypeptide toxins (33). This is certainly true of the conotoxins where functional diversity is achieved by a combination of sequence variation and structural variation. As a result, structural analysis reveals few clues as to the potential molecular target of a given polypeptide. Fig. 5 shows ribbon representations of several conotoxin structures that contain six Cys residues and exhibit the same disulfide-bonding pattern exhibited by gm9a, namely C_1-C_4/C_2-C_5/C_3-C_6. Further details of these conopeptides are given in Table II.

μ-GIIIA, μ-GIIIB, and ψ-PIIIE (Fig. 5, *A*, *B*, and *C*, respectively, and Table II) all share a common Cys framework (-$CCX_{4-5}CX_{4-5}CX_4$CC-) and the C_1-C_4/C_2-C_5/C_3-C_6 bonding pattern (2). These polypeptides are similarly structured but functionally distinct. The μ-conotoxins bind selectively to sodium channels (34, 35, 44), and ψ-PIIIE inhibits the acetylcholine receptor (36). An analogous situation exists among the ω- and κ-O-superfamily conotoxins (Fig. 5, *H–K*). All of these polypeptides exhibit the ICK motif within the same Cys framework (-$CX_6CX_6CCX_{2-3}CX_{4-6}$C-), and despite significant sequence diversity, even among the ω-conotoxins, all have a remarkably similar structure. However, the ω-conotoxins SO3 (*H*), MVIIA (*I*), and GVIA (*J*) all selectively inhibit voltage-gated calcium channels (41, 42), and PVIIA (*K*), a κ-conotoxin, selectively inhibits Shaker potassium channels (43). In contrast is conotoxin GS (*E*), which is structurally related to the O-conotoxins through a common Cys framework and ICK motif but is functionally related to the μ-conotoxins as it binds competitively with μ-GIIIA to skeletal muscle sodium channels (38). This is complicated further by the fact that conotoxin GS has low sequence identity with either GIIIA or GIIIB and is 50% larger.

Structural Diversity within Superfamilies—Despite having a Cys framework in common, there can also be significant structural diversity among members of a given superfamily. This diversity can be attributed mainly to the different inter-cysteine spacings across the sequences and is well illustrated by considering the structural variation among the O-superfamily polypeptides (Fig. 5, *D–K*), all of which have a common Cys framework and exhibit the ICK motif.

There is significant sequence variation among ω-SO3 (Fig. 5, *H*), ω-MVIIA (*I*), ω-GVIA (*J*), and κ-PVIIA (*K*), even though they have very similar structures. An inspection of Table II shows that the number of residues between sequential cysteines is reasonably consistent across the four polypeptides, *i.e.* 6 (C_1-C_2), 6 (C_2-C_3), 0 (C_3-C_4), 2–3 (C_4-C_5), and 4–6 (C_5-C_6). By contrast, conotoxin GS (*E*) has inter-cysteine spacings of 6, 3, 0,

TABLE II
Description of various conopeptides that have the same disulfide-bonding pattern as gm9a

Peptide	Sequence[a]		$C_x - C_{x+1}$[b]	Ref.
A-GIIIB	RDCCTXXRKCKDRRCKXMKCCA	*Conus geographus*	0, 5, 4, 4, 0	(34)
B-GIIIA	RDCCTXXKKCKDRQCKXQRCCA	*C. geographus*	0, 5, 4, 4, 0	(35)
C-PIIIE	HXXCCLYGKCRRYXGCSSASCCQR	*Conus purpurascens*	0, 4, 5, 4, 0	(36)
D-TVIIA	SCSGRDSRCXXVCCMGLMCSRGKCVSIYGE	*Conus tulipa*	6, 3, 0, 4, 4	(37)
E-GS	ACSGRGSRCXXQCCMGLRCGRGNPQKCIGAHγDV	*C. geographus*	6, 3, 0, 4, 7	(38)
F-EVIA$_{trans}$	DDCIKXYGFCSLPILKNGLCCSGACVGVCADL	*Conus ermineus*	6, 9, 0, 3, 3	(PDB 1GIP)
G-EVIA$_{cis}$	DDCIKXYGFCSLPILKNGLCCSGACVGVCADL	*C. ermineus*	6, 9, 0, 3, 3	(PDB 1GIZ)
H-SO3	CKAAGKPCSRIAYNCCTGSCRSGKC	*C. striatus*	6, 6, 0, 3, 4	(PDB 1FYG)
I-MVIIA	CKGKGAKCSRLMYDCCTGSCRSGKC	*Conus magus*	6, 6, 0, 3, 4	(41)
J-GVIA	CKSXGSSCSXTSYNCCRSCNXYTKRCY	*C. geographus*	6, 6, 0, 2, 6	(42)
K-PVIIA	CRIXNQKCFQHLDDCCSRKCNRFNKCV	*C. purpurascens*	6, 6, 0, 3, 5	(43)
L-gm9a	SCNNSCQSHSDCASHCICTFRGCGAVN	*C. gloriamaris*	3, 5, 3, 1, 4	(1)
M-tx9a	SCNNSCQγHSDCγSHCICTFRGCGAVN	*C. textile*	3, 5, 3, 1, 4	(1)

[a] Cysteines are shown emboldened, residues with charged side chains at physiological pH are underlined, γ represents Gla, and X represents hydroxyprolines.
[b] Each number series refers to the number of residues between sequential cysteines in the polypeptide sequence *i.e.* the number of residues between C_1 and C_2, C_2 and C_3, C_3 and C_4, C_4 and C_5, and C_5 and C_6.

4, and 7 and a structure that differs from the ω- and κ-conotoxins. In TVIIA (*D*), these spacings are 6, 3, 0, 4, and 4, and as a consequence, it has essentially the same structure as conotoxin GS over the disulfide-linked region of the molecule with the exception that the loop between C_5 and C_6 is approximately half as large in TVIIA (Fig. 5). A similarly significant departure from the classic ω-conotoxin fold is observed in EVIA (*G*), which has the spacings of 6, 9, 0, 3, and 3. When this type of analysis is applied to the P-conotoxin gm9a in which 3, 5, 3, 1, and 4 residues separate sequential Cys residues, it is readily apparent why the structure of this polypeptide is unique among those shown in Fig. 5.

In light of this analysis, two points can be made with regard to the newly defined P-conotoxins. First, because the number of residues between sequential half-cystines is a significant indicator of structural variation and as new members of this family of conopeptides are identified, this source of structural diversity can be used to assess the extent of their homology with gm9a. Second, because the P-conotoxins have no cysteines directly adjacent to one another, the scaffold underlying this superfamily of polypeptides has the greatest scope for exhibiting structural and functional diversity among all of the six Cys-containing conotoxins. This latter point has significant implications for protein engineering and functional epitope mimicry (40, 45). An inspection of the structure of gm9a suggests that the loops between the second and third half-cysteines and the fifth and sixth are potentially the most suitable for the introduction of new sequences.

Implications for tx9a from C. textile—Chemically synthesized gm9a, the *C. gloriamaris* spasmodic peptide, has biological activity comparable to that elicited by the *C. textile* spasmodic peptide in an *in vivo* assay in mice (1). The two spasmodic peptide sequences from *C. textile* (tx9a) and *C. gloriamaris* (gm9a) differ in only three positions, with Ser^1, Ser^8, and Ala^{13} in gm9a substituted for Gly, Gla, and Gla, respectively, in tx9a. We expect tx9a to adopt a conformation similar to that of gm9a, because the location of the six Cys residues is identical in the two polypeptides, the substitution at the flexible N terminus is not likely to be structurally significant, and the two Gla substitutions involve neither glycine nor proline residues, mutations that might be expected to yield structural variation. In addition, it was demonstrated by Hill *et al.* (38) that substituting Gla for Glu in conotoxin GS resulted in no change in the backbone conformation of that polypeptide.

The nature of the molecular target of gm9a and tx9a remains undefined, but the symptomatology elicited by both polypeptides is reminiscent of spasmodic and spastic mouse mutants (3, 4), which were characterized as being defective in glycine receptors. Although the receptor for these polypeptides is still to be determined, it is apparent from the comparable results of the mouse assays that the two γ-carboxyglutamates in tx9a are not involved directly in receptor binding.

An analysis of the gm9a structure shows that residues 8 and 13 (Fig. 4*F*) are found on the same face of the molecule, flanking the only acidic residue Asp^{11}. One consequence of this finding is that on one face of the molecule, tx9a is substantially more electronegative than is gm9a. This is significant because in the main, conotoxins are rich in basic side-chains (see Table II) that interact with anionic sites in their ion channel receptors. This also implies that this region of the molecular surface does not constitute the receptor-binding interface of these polypeptides. Rather, it can be inferred that the polar face of these molecules is solvent-exposed when the polypeptides bind their target and that the binding epitope is probably on the hydrophobic/cationic face of the molecule.

γ-Carboxyglutamates have been implicated in Ca^{2+} binding by Prorok *et al.* (39), who demonstrated that the Gla-rich *Conus*-derived conantokins T and G were susceptible to conformational change as a result of calcium binding to Gla residues. In these polypeptides, however, Gla residues are in close proximity to one another with some being adjacent in the sequences. Hill *et al.* (38) considered the possibility that the single Gla residue in conotoxin GS might be involved in Ca^{2+} binding. They demonstrated by NMR that there was no conformational change in the polypeptide observable in the presence of calcium ions and found no evidence of line broadening or perturbation of Gla^{32} side-chain resonances that might indicate calcium binding. It was concluded that this single residue might not play a crucial role in either the structure or function of conotoxin GS.

tx9a has two Gla residues, but inspection of the gm9a structures indicates that across the family of 20 structures, residues 8 and 13 are always >10-Å apart. Clearly, this is too large a distance for these residues to cooperatively chelate Ca^{2+} ions in the folded structure. However, it is conceivable that one or other of the Gla residues and the intervening Asp^{11} could participate in Ca^{2+} binding in tx9a. It is also possible that these Gla residues could be involved in the folding of the tx9a polypeptide. Prorok *et al.* (39) found that Ca^{2+} binding induced an increase in the α-helical content of the conantokins considered in their work. In gm9a and presumably in tx9a, residues 8 and 13 are found in the loops of the molecule. In tx9a, the formation of these loops could conceivably be induced by Ca^{2+} binding.

Acknowledgments—We thank Richard DelaCruz for preparation of synthetic polypeptide for NMR work and Elsie Jimenez for bioassays.

REFERENCES

1. Lirazan, M. B., Hooper, D., Corpuz, G. P., Ramilo, C. A., Bandyopadhyay, P., Cruz, L. J., and Olivera, B. M. (2000) *Biochemistry* **39,** 1583–1588
2. Balaji, R. A., Ohtake, A., Sato, K., Gopalakrishnakone, P., Kini, R. M., Seow, K. T., and Bay, B. H. (2000) *J. Biol. Chem.* **275,** 39516–39522
3. Ryan, S. G., Buckwalter, M. S., Lynch, J. W., Handford, C. A., Segura, L., Shiang, R., Wasmuth, J. J., Camper, S. A., Schofield, P., and O'Connell, P. (1994) *Nat. Genet.* **7,** 131–135
4. Saul, B., Schmieden, V., Kling, C., Mulhardt, C., Gass, P., Kuhse, J., and Becker, C. M. (1994) *FEBS Lett.* **350,** 71–76
5. Pallaghy, P. K., and Norton, R. S. (2000) *Biopolymers* **54,** 173–179
6. Norton, R. S., Pallaghy, P. K., Baell, J. B., Wright, C. E., Lew, M. J., and Angus, J. A. (1999) *Drug Dev. Res.* **46,** 206–218
7. Norton, R. S., and Pallaghy, P. K. (1998) *Toxicon* **36,** 1573–1583
8. Wishart, D. S., Bigam, C. G., Yao, J., Abildgaard, F., Dyson, H. J., Oldfield, E., Markley, J. L., and Sykes, B. D. (1995) *J. Biomol. NMR* **6,** 135–140
9. Marion, D., and Wüthrich, K. (1983) *Biochem. Biophys. Res. Commun.* **113,** 967–974
10. Sklenar, V., Piotto, M., Leppik, R., and Saudek, V. (1993) *J. Magn. Reson.* **102,** 241–245
11. Kumar, A., Ernst, R. R., and Wüthrich, K. (1980) *Biochem. Biophys. Res. Commun.* **95,** 1–6
12. Braunschweiler, L., and Ernst, R. R. (1983) *J. Magn. Reson.* **53,** 521–528
13. Levitt, M. H., Freeman, R., and Frenkiel, T. (1983) *Adv. Magn. Reson.* **11,** 47
14. Rance, M., Sørensen, O. W., Bodenhausen, G., Wagner, G., Ernst, R. R., and Wüthrich, K. (1983) *Biochem. Biophys. Res. Commun.* **117,** 479–485
15. Griesinger, C., Sørensen, O. W., and Ernst, R. R. (1987) *J. Magn. Reson.* **75,** 474–492
16. Bartels, C., Xia, T. H., Billeter, M., Güntert, P., and Wüthrich, K. (1995) *J. Biomol. NMR* **6,** 1–10
17. Güntert, P., Mumenthaler, C., and Wüthrich, K. (1997) *J. Mol. Biol.* **273,** 283–298
18. Brunger, A. T., Adams, P. D., Clore, G. M., DeLano, W. L., Gros, P., Grosse-Kunstleve, R. W., Jiang, J. S., Kuszewski, J., Nilges, M., Pannu, N. S., Read, R. J., Rice, L. M., Simonson, T., and Warren, G. L. (1998) *Acta Crystallogr. Sec. D* **54,** 905–921
19. Linge, J. P., and Nilges, M. (1999) *J. Biomol. NMR* **13,** 51–59
20. Laskowski, R. A., Rullmannn, J. A., MacArthur, M. W., Kaptein, R., and Thornton, J. M. (1996) *J. Biomol. NMR* **8,** 477–486
21. Gray, W. R. (1993) *Protein Sci.* **2,** 1732–1748
22. Seavey, B. R., Farr, E. A., Westler, W. M., and Markley, J. L. (1991) *J. Biomol. NMR* **1,** 217–236
23. Pallaghy, P. K., Nielsen, K. J., Craik, D. J., and Norton, R. S. (1994) *Protein Sci.* **3,** 1833–1839
24. Baxter, N. J., and Williamson, M. P. (1997) *J. Biomol. NMR* **9,** 359–369
25. Berman, H. M., Westbrook, J., Feng, Z., Gilliland, G., Bhat, T. N., Weissig, H., Shindyalov, I. N., and Bourne, P. E. (2000) *Nucleic Acids Res.* **28,** 235–242
26. Kabsch, W., and Sander, C. (1983) *Biopolymers* **22,** 2577–2637
27. *BioMagResBank (BMRB)* database. www.bmrb.wisc.edu
28. Bundi, A., and Wüthrich, K. (1979) *Biopolymers* **18,** 285–297
29. Tanokura, M., Tasumi, M., and Miyazawa, T. (1976) *Biopolymers* **15,** 393–401
30. Perutz, M. F., Gronenborn, A. M., Clore, G. M., Fogg, J. H., and Shih, D. T. (1985) *J. Mol. Biol.* **183,** 491–498
31. Shire, S. J., Hanania, G. I., and Gurd, F. R. (1974) *Biochemistry* **13,** 2967–2974
32. Keim, P., Vigna, R. A., Morrow, J. S., Marshall, R. C., and Gurd, F. R. (1973) *J. Biol. Chem.* **248,** 7811–7818
33. Norton, R. S. (2002) in *Perspectives in Molecular Toxinology* (Ménez, A., ed) pp. 159–173, John Wiley & Sons, Inc., New York
34. Wakamatsu, K., Kohda, D., Hatanaka, H., Lancelin, J. M., Ishida, Y., Oya, M., Nakamura, H., Inagaki, F., and Sato, K. (1992) *Biochemistry* **31,** 12577–12584
35. Hill, J. M., Alewood, P. F., and Craik, D. J. (1996) *Biochemistry* **35,** 8824–8835
36. Mitchell, S. S., Shon, K. J., Foster, M. P., Davis, D. R., Olivera, B. M., and Ireland, C. M. (1998) *Biochemistry* **37,** 1215–1220
37. Hill, J. M., Alewood, P. F., and Craik, D. J. (2000) *Eur. J. Biochem.* **267,** 4649–4657
38. Hill, J. M., Alewood, P. F., and Craik, D. J. (1997) *Structure* **5,** 571–583
39. Prorok, M., Warder, S. E., Blandl, T., and Castellino, F. J. (1996) *Biochemistry* **35,** 16528–16534
40. Mourier, G., Servent, D., Zinn-Justin, S., and Ménez, A. (2000) *Protein Eng.* **13,** 217–225
41. Nielsen, K. J., Thomas, L., Lewis, R. J., Alewood, P. F., and Craik, D. J. (1996) *J. Mol. Biol.* **263,** 297–310
42. Pallaghy, P. K., and Norton, R. S. (1999) *J. Pept. Res.* **53,** 343–351
43. Savarin, P., Guenneugues, M., Gilquin, B., Lamthanh, H., Gasparini, S., Zinn-Justin, S., and Ménez, A. (1998) *Biochemistry* **37,** 5407–5416
44. Sato, K., Ishida, Y., Wakamatsu, K., Kato, R., Honda, H., Ohizumi, Y., Nakamura, H., Ohya, M., Lancelin, J. M., Kohda, D., and Inagaki, F. (1991) *J. Biol. Chem.* **266,** 16989–16991
45. Vita, C., Drakopoulou, E., Vizzavona, J., Rochette, S., Martin, L., Ménez, A., Roumestand, C., Yang, Y. S., Ylisastigui, L., Benjouad, A., and Gluckman, J. C. (1999) *Proc. Natl. Acad. Sci. U. S. A.* **96,** 13091–13096